ADVANCED MATERIALS
www.advmat.de

Materials Views
www.MaterialsViews.com

Adjustable Zero Thermal Expansion in Antiperovskite Manganese Nitride

Xiaoyan Song, Zhonghua Sun, Qingzhen Huang, Markus Rettenmayr, Xuemei Liu, Martin Seyring, Guannan Li, Guanghui Rao, and Fuxing Yin*

It is general knowledge that materials expand with increasing temperature and contract with decreasing temperature. Only few materials seem to neither expand nor contract over a certain temperature range and thus feature near zero thermal expansion (ZTE) behavior. These materials are the focus of recent scientific work[1–5] and have potential technical applications in both structural materials, e.g., precision engineered parts, microdevices, and systems that are subject to thermal shock, and functional materials, e.g., thermomechanical actuators. In most cases ZTE materials are based on a composite, combining positive thermal expansion (PTE) and negative thermal expansion (NTE) behavior.[6–10] In addition to the Invar effect in Fe-Ni alloys,[11] ZTE in a single material has, to date, only been documented in a small number of compounds such as YbGaGe,[2] Mn_3AN (A = Cu/Sn, Zn/Sn),[12] $Fe[Co(CN)_6]$,[13] and $N(CH_3)_4CuZn(CN)_4$.[14] Among the candidates for ZTE materials, the antiperovskite manganese nitrides are prominent, due to their special spectrum of properties including ZTE isotropy,[12] electric conductivity,[15] and good mechanical performance.[16] However, the antiperovskite manganese nitrides show relatively narrow ZTE temperature ranges, generally less than 80 K.[12]

Prof. X. Song, Dr. Z. Sun, Dr. X. Liu
College of Materials Science and Engineering
Key Laboratory of Advanced Functional Materials
Education Ministry of China
Beijing University of Technology
Beijing 100124, China,
E-mail: xysong@bjut.edu.cn
Q. Huang, G. Li
NIST Center for Neutron Research
National Institute of Standards and Technology
Gaithersburg MD, 20899-6102, USA
Prof. M. Rettenmayr, Dr. M. Seyring
Institute of Materials Science and Technology
Metallic Materials
Friedrich-Schiller University of Jena
07743 Jena, Germany
G. Li, Prof. G. Rao
Institute of Physics
Chinese Academy of Sciences
Beijing 100190, China
Prof. F. Yin
Innovative Materials Engineering Laboratory
National Institute for Materials Science
Tsukuba, Ibaraki 305-0047, Japan

DOI: 10.1002/adma.201102552

It has been attempted in the past to influence the NTE or ZTE temperature range of antiperovskite manganese nitrides by adding various alloying elements,[8,12] which mostly led to a shift in the (still limited) temperature range. Although the NTE and ZTE are considered to be a magneto-elastic effect,[7,8] the precise mechanism based on which the thermal expansion behavior can be controlled has remained unclear. This may be the reason why drastic changes in the NTE or ZTE properties of antiperovskite manganese nitrides were not achieved. Here we focus on the ZTE mechanism through which the ZTE temperature range of antiperovskite manganese nitride is extended remarkably by modulating the atomic site occupancy that in turn controls the magnetic ordering transition in the material.

Three different microstructures were prepared in the present experiments as consolidated antiperovskite manganese nitrides $Mn_3Cu_{0.5}Ge_{0.5}N$: coarse-grained polycrystalline (mean grain size ≈2.0 μm), nanocrystalline (mean grain size ≈30 nm), and ultra-nanocrystalline (mean grain size ≈12 nm, **Figure 1**a). All the microstructures have the same phase constitution with an antiperovskite Mn_3CuN-type structure (for details see the Supporting Information, Figure S1), and no phase transformation was found in the investigated temperature range. The characteristics of the nanograins in the ultra-nanocrystalline material are illustrated by electron diffraction pattern and high-resolution transmission electron microscopy (TEM; Figure 1a–c). The crystal and magnetic structures were refined using neutron powder diffraction intensity data (see Supporting Information, Figure S1). Details of the cubic antiperovskite structure of $Mn_3Cu_{0.5}Ge_{0.5}N$ are shown in Figure 1d. The structure has a *P m-3m* symmetry and the Cu/Ge, N and Mn atoms are at sites 1*a* (0,0,0), 1*b* (½,½,½) and 3*c* (0,½,½), respectively. The magnetic structure is shown in Figure 1e, as a rhombohedral setting with symmetry of the magnetic Shubnikov group *R-3* and a lattice $a_H = b_H = \sqrt{2}a$ and $c_H = \sqrt{3}a$, where a_H, b_H, and c_H are the rhombohedron lattice parameters with a hexagonal setting and *a* is the cubic lattice parameter of the ultra-nanocrystalline $Mn_3Cu_{0.5}Ge_{0.5}N$.

By careful structure analysis (see Supporting Information, Table S1,S2) we found that the Mn atoms mix with Cu/Ge atoms and vacancies at the 3*c* site, as shown in **Table 1**. The Mn occupancy at the 3*c* sites decreases from 100% in the coarse-grained to ≈87.8% in the nanocrystalline to ≈78.7% in the ultra-nanocrystalline material. Correspondingly, the three materials with different microstructural length scales are denoted as Mn 1000, Mn 878, and Mn 787, respectively. The 1*a* and 1*b* sites are fully occupied by Cu/Ge and N, respectively. Thus, there is clear evidence that at a given composition, nanostructuring

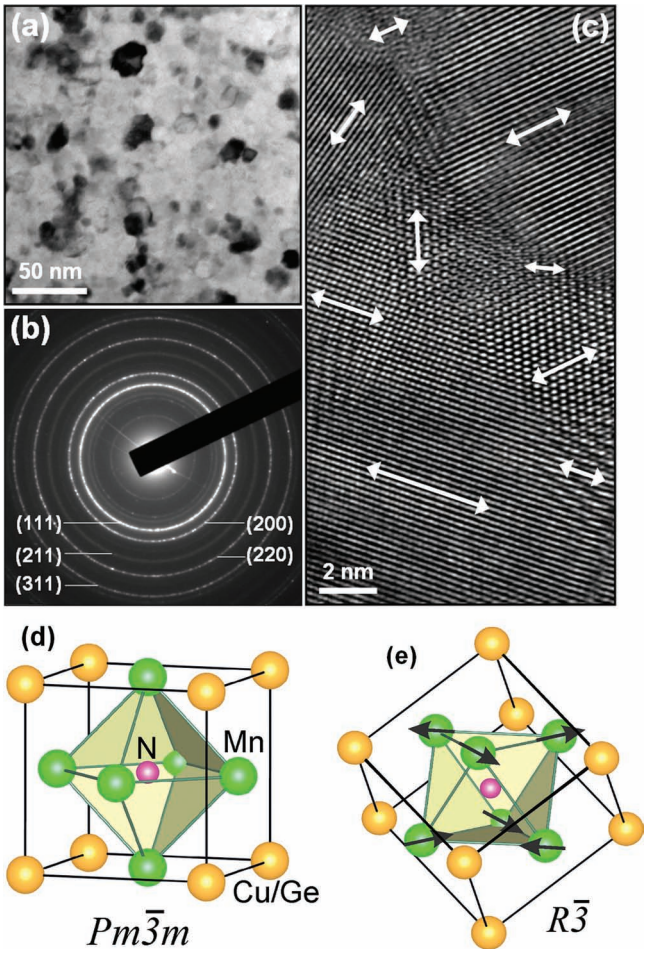

Figure 1. Microstructural details of ultrananocrystalline $Mn_3Cu_{0.5}Ge_{0.5}N$. a) Overview of morphology of nanograins. b) Electron diffraction pattern with indexing. c) High-resolution TEM image of nanograin structure. The arrows represent the orientations of the visible lattice planes in the nanograins. d) Cubic antiperovskite crystal structure obtained from refinement of neutron powder diffraction intensity data. e) Magnetic structure proposed from refinement of neutron powder diffraction intensity data. The arrows indicate the magnetic moment directions.

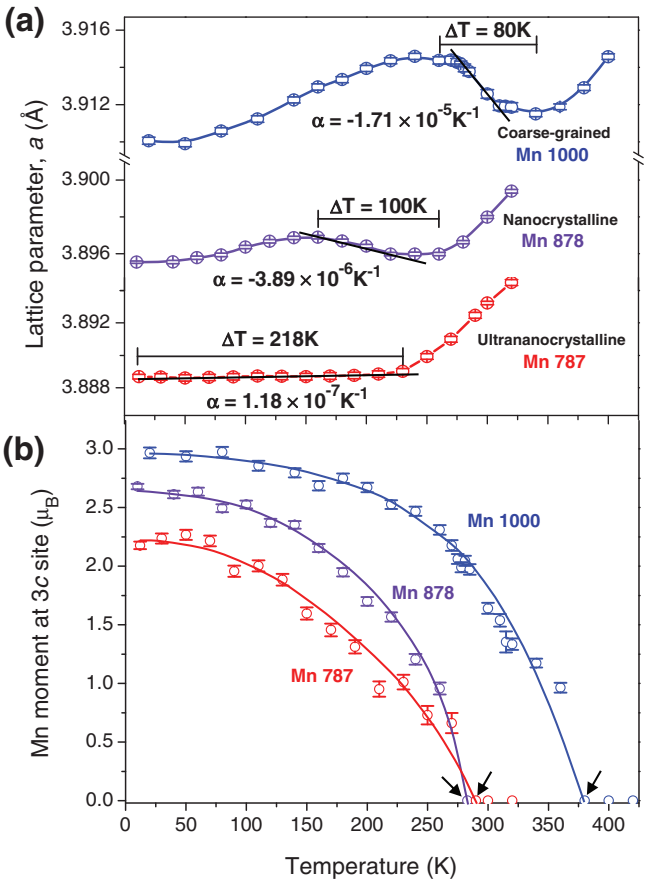

Figure 2. Temperature dependence of lattice parameter and Mn magnetic moment of $Mn_3Cu_{0.5}Ge_{0.5}N$. a) Thermal expansion behavior of three materials having different microstructural length scales. b) Magnetic moments of the three materials as a function of temperature. The arrows indicate the magnetic ordering transition temperatures. The error bars in the figures indicate the standard deviation.

of the materials reduces the Mn site occupancy in the antiperovskite manganese nitrides.

The variations of the cubic lattice parameter a and magnetic moments at 3c sites as a function of temperature are shown in **Figure 2**. In Figure 2a, the distinctly different characteristics of the thermal expansion behavior of the three materials are clearly visible. For the coarse-grained material with a Mn site occupancy of 100% (denoted as Mn 1000), a increases with decreasing temperature from 340 K to 260 K (where a reaches a maximum), indicating the NTE behavior in a temperature range of $\Delta T = 80$ K (260–340 K) with a negative linear expansion coefficient of $\alpha = -1.71 \times 10^{-5}$ K^{-1}, as depicted by the solid line. The nanocrystalline material with a Mn site occupancy of 87.8% (denoted as Mn 878) also exhibits NTE behavior. The temperature range is, however, extended to $\Delta T = 100$ K (160–260 K). The negative linear expansion coefficient is $\alpha = -3.89 \times 10^{-6}$ K^{-1}, which is significantly lower than that of the Mn 1000 material. For the ultra-nanocrystalline material, which has a Mn site occupancy of 78.7% (denoted as Mn 787), the lattice parameter a is essentially constant below 230 K, within a considerably wide temperature range of $\Delta T = 218$ K (12–230 K). A minuscule thermal expansion coefficient $\alpha = 1.18 \times 10^{-7}$ K^{-1} is found below 230 K, demonstrating the ZTE behavior in the Mn 787 material. In comparison,

Table 1. Lattice structure parameters of $Mn_3Cu_{0.5}Ge_{0.5}N$ with different microstructural length scales. Errors are given in parentheses.

Microstructure	Coarse-grained	Nanocrystalline	Ultrananocrystalline
Mn/CuGe/vacancy occupancy	1.000(1)/0.0/0.0	0.878(4)/0.041/0.082	0.787(4)/0.071/0.142
Sample designation	Mn 1000	Mn 878	Mn 787
Lattice parameter at room temperature [Å]	3.91211(9)	3.89799(7)	3.89332(7)
Mn magnetic moment at low temperature [μ_B]	2.97(5)	2.71(2)	2.22(3)

the characteristic temperature range reported in the discovery of ZTE in the antiperovskite manganese nitrides is ≈50 K to 80 K.[12] Thus, a drastically extended ZTE temperature range that is 3 to 4 times larger was obtained in the ultra-nanocrystalline $Mn_3Cu_{0.5}Ge_{0.5}N$, which can be called a form of giant ZTE. The dependence of the NTE or ZTE temperature range of antiperovskite manganese nitrides on the lattice site occupancy demonstrates the potential for designing new applications in a variety of structural and functional materials.

Along with the difference in the thermal expansion behavior of the three materials, the magnetic moment was observed to decrease from Mn 1000 to Mn 878 to Mn 787 in the entire observed temperature range, as shown in Figure 2b. Comparison of Figure 2a,b shows that the NTE or ZTE behavior only occurs below the magnetic ordering transition temperature. This confirms the strong coupling of the thermal expansion behavior with the magnetic ordering process that takes place over a temperature range.

To explore the correlation between the magnetic ordering and the thermal expansion properties unambiguously, the rates of change of the magnetic moment (dM/dT) and the lattice parameter (da/dT) with temperature were studied for the three materials, as shown in **Figure 3**. It is observed that below the magnetic ordering transition temperature (marked by the vertical arrow), the rate of change of the lattice parameter with respect to temperature (da/dT) is mainly affected by the rate of change of the magnetic moment (dM/dT). In the temperature range where $da/dT \leq 0$ (i.e., in the presence of NTE or ZTE), as indicated by the slope triangles in Figure 3, the rate of change of dM/dT with respect to temperature decreases clearly from Mn 1000 to Mn 878 to Mn 787, with values of 0.18, 0.11, and 0.05, respectively. Similarly, the change rate of the lattice parameter with respect to temperature decreases in the order from Mn 1000 to Mn 878 to Mn 787. This shows that the decrease of the Mn site occupancy significantly affects the magnetic ordering rate with temperature in the material. The same tendency is observed for the rate of change of the lattice parameter with respect to temperature for the different materials. The results show that below the magnetic ordering transition temperature, da/dT is controlled by dM/dT.

To understand more profoundly the process that the magnetic ordering induces lattice expansion, it is indispensable to quantify the degree to which the magnetic ordering contributes to the lattice expansion. In the present experiments, characterization of the magnetic ordering effect was performed for Mn 787 by the neutron powder diffraction under a high pressure of 0.55 GPa, which was applied in order to hinder the magnetic ordering and then to observe the change of the thermal expansion behavior. Under high pressure with the weakening of magnetic ordering (**Figure 4**a), in contrast to the ZTE behavior observed at atmospheric pressure, ordinary PTE behavior is found (Figure 4b). Thus, the impact of magnetic ordering on the lattice expansion, i.e., the NTE effect, is distinguished and can be quantified by comparing the measured ZTE and PTE with respect to the change of the magnetic moment (Supporting Information, Figure S2).

The different thermal expansion features shown in the three materials are attributed to the difference in their magnetic ordering processes. The Mn occupancy at its lattice

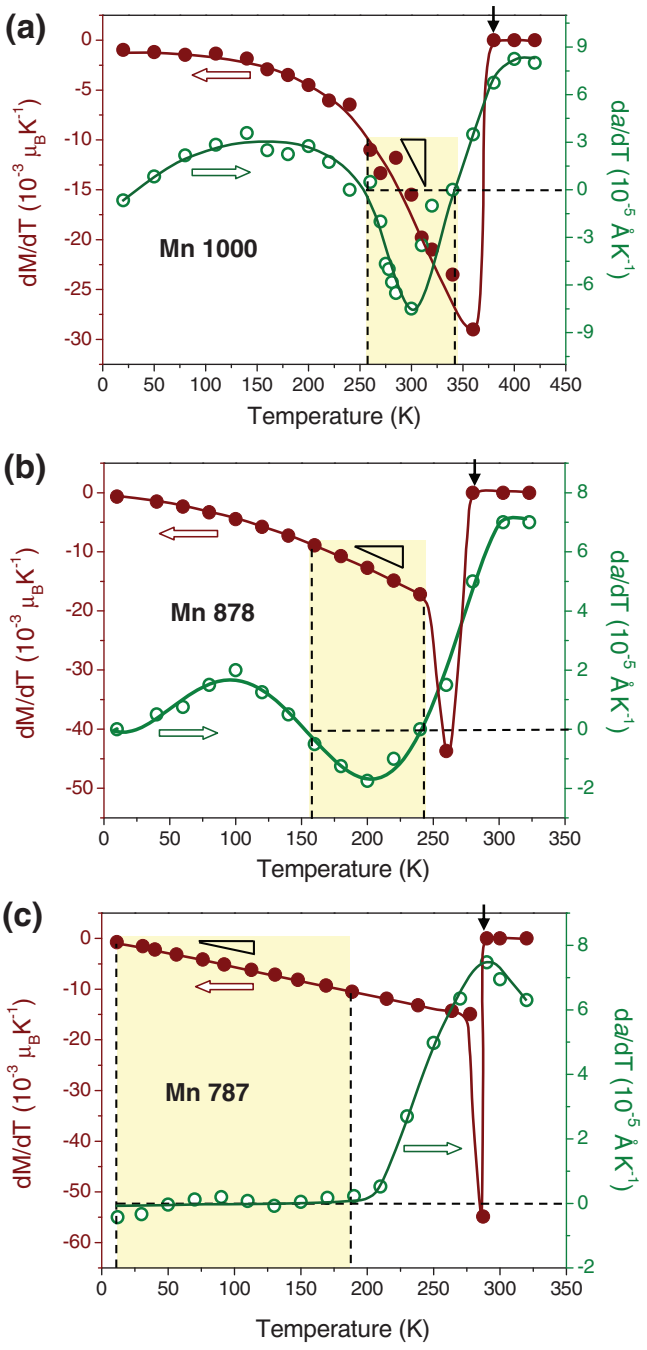

Figure 3. Rate of change of the magnetic moment and lattice parameter with respect to temperature: a) Mn 1000, b) Mn 878, and c) Mn 787. The vertical arrows indicate the magnetic ordering transition temperatures. The slope triangles reflect the changes of dM/dT with respect to temperature in the range where $da/dT \leq 0$ (i.e., in the presence of NTE or ZTE).

sites decreases with the decrease of the grain size, which is a consequence of the increased density of the crystal defects and lattice distortion due to the nanostructuring. The Mn occupancy affects the magnetic moment and the lattice parameter of the material prominently, as shown in Figure 4c. The magnetic moment decreases drastically with the decrease in Mn occupancy. The low Mn site occupancy in the

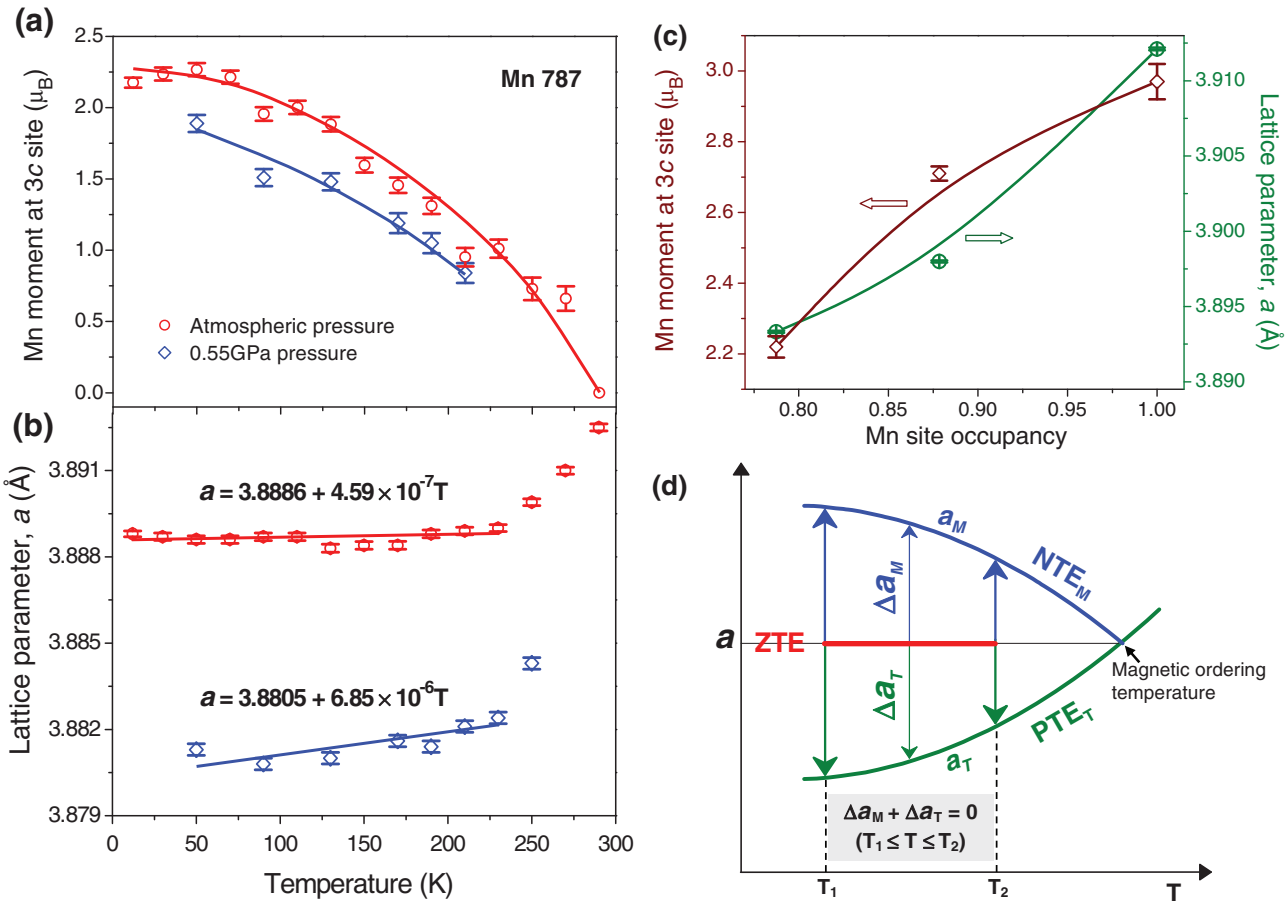

Figure 4. Mechanism for occurrence of ZTE. a) Decrease of magnetic moment under high pressure. b) Change of the temperature dependence of the lattice parameter under high pressure. While ZTE behavior is observed at atmospheric pressure, ordinary PTE behavior is found under high pressure when the magnetic ordering is hindered. c) Dependence of the magnetic moment and lattice parameter on the Mn site occupancy. d) Mechanism for the occurrence of ZTE. NTE_M and PTE_T denote NTE caused by magnetic ordering and PTE caused by temperature, respectively, and a_M and a_T are the corresponding lattice parameters. Δa_M and Δa_T are the changes in the lattice parameter caused by magnetic ordering and temperature, respectively. In the temperature range between T_1 and T_2 where $\Delta a_M + \Delta a_T = 0$, the ZTE behavior occurs.

ultra-nanocrystalline material (Mn 787) leads to a low magnetic ordering transition temperature (Figure 2b), a small magnetic moment (Figure 2b and Figure 4c), and a low rate of increase in the magnetic moment upon cooling (Figure 3c). These result in the decrease of both the degree and the rate of the magnetic ordering with temperature. Based on the experimental results, the mechanism of ZTE occurring in Mn 787 is suggested as follows (see Figure 4d). Below the magnetic ordering transition temperature, NTE is induced, as denoted by NTE_M in Figure 4d, leading to an expanding lattice parameter a_M. When the lattice expansion induced by the magnetic ordering, Δa_M, is larger than the thermal contraction due to the temperature decrease (as denoted by PTE_T), Δa_T, the NTE behavior appears. However, due to the reduced degree of the magnetic ordering caused by the low Mn occupancy at its lattice sites, the lattice expansion compensates the thermal contraction, i.e., in a certain temperature range $\Delta T = T_2 - T_1$, there is $\Delta a_M + \Delta a_T = 0$, thus ZTE behavior is observed. Furthermore, due to the low rate of the magnetic ordering with temperature in the material, the equivalent compensation persists over a wide temperature range, yielding "giant" ZTE.

From the variation in the thermal expansion behavior observed in antiperovskite manganese nitrides, it is clear that the Mn site occupancy in the antiperovskite crystal structure plays a dominant role in controlling the magnetic ordering process. This elucidates that modulating the atom occupancy at certain lattice sites in a magnetic structure, independently of the manufacturing process, can control the magnetic ordering and hence tailor both the thermal expansion behavior and its operating temperature range. At a given composition as in the present experiments, a low Mn site occupancy can be obtained by nanostructuring the material. Then the degree and the rate of magnetic ordering are both reduced in the nanocrystalline structure as compared to those in the coarse-grained structure. When the Mn site occupancy is reduced below a critical value, e.g., as that in the ultra-nanocrystalline material (Mn 787), the lattice expansion induced by the weakened magnetic ordering compensates the thermal contraction upon cooling. This process advances slowly with temperature decrease due to the low magnetic ordering rate with temperature. As a result, ZTE with a wide temperature range is achieved in the ultra-nanocrystalline material. It should be noted that owing to the

superposition of the two effects of NTE_M and PTE_T and despite being below the magnetic ordering transition temperature, PTE will appear where the thermal contraction cannot be compensated by the lattice expansion, as observed in the temperature range 230–290 K for the ultra-nanocrystalline material (Figure 2a). The antiperovskite manganese nitride thus can exhibit PTE, NTE, or ZTE behavior in its pure form, depending on the relative magnitudes of the thermal contraction and the magnetic ordering induced lattice expansion (see demonstration in the Supporting Information, Figure S3).

It is worth noting that adjusting the thermal expansion properties of the crystalline components also sets the corresponding properties of the bulk material containing interfaces (e.g., grain boundaries). Applying the mechanism found in the present work, the NTE of the crystalline components can be designed and controlled such that the entire bulk material (e.g., a candidate for high precision devices) has negligible thermal expansion.

In summary, we present the first clear experimental evidence for mechanisms of NTE and ZTE and how to control them both on an atomic scale and for the bulk materials including interfaces. The major finding is that the thermal expansion behavior of the antiperovskite manganese nitrides can be controlled by modulating the Mn occupancy at its lattice sites. The Mn site occupancy dominates the degree and rate of the magnetic ordering with temperature and hence the amount and rate of NTE with temperature. Applying this mechanism, ZTE over a temperature range larger by a factor of three to four than that reported so far for the antiperovskite manganese nitrides is achieved in an ultra-nanocrystalline structure with a reduced Mn site occupancy. We conclude that it is a universal mechanism that adjusting the atom occupancy in a magnetic structure, independently of the manufacturing process, can precisely tailor the thermal expansion behavior and its operating temperature range for all the materials that feature magneto-elastic behavior. It is thus anticipated that new varieties of ZTE materials can be designed based on this mechanism.

Experimental Section

Materials Synthesis: All processing steps were performed in an in-house-built "oxygen-free" in situ fabrication system,[17,18] which combines powder treatment with spark plasma sintering in an entirely closed system filled with highly purified nitrogen. The coarse-grained polycrystalline $Mn_3Cu_{0.5}Ge_{0.5}N$ material was prepared by sintering the $Mn_2N_{0.86}$,[19] Cu, and Ge powders with a final temperature of 973 K for 10 min. The nanocrystalline and ultra-nanocrystalline $Mn_3Cu_{0.5}Ge_{0.5}N$ materials were prepared starting from the coarse-grained material. By milling with ball-to-powder ratios of 20:1 and 30:1 for 20 h and 30h, respectively, powders with nanocrystalline and amorphous structures were produced. Then the powders were sintered separately using constant pressures (300 and 500 MPa, respectively) and a final temperature of 773 K for 3 min.

Characterization: The mean grain sizes of the nanocrystalline and ultra-nanocrystalline materials were measured in the transmission electron microscope with a recently developed method to separate overlapping grains and to determine the size distribution with sufficient statistics.[20,21] The neutron powder diffraction experiments were performed at the NIST Center for Neutron Research on the BT-1 high-resolution neutron powder diffractometer. The measuring temperatures were between 20 K and 420 K for the coarse-grained material and between 10 K and 320 K for the nanocrystalline and ultra-nanocrystalline materials, respectively. Measurements at a pressure of 0.55 GPa were also carried out with helium gas as pressure medium. The crystal and magnetic structures were refined by the Rietveld method using the General Structure Analysis System (GSAS) suite of programs.[22]

Supporting Information

Supporting Information is available from the Wiley Online Library or from the author.

Acknowledgements

This work was supported by the Chinese National Programs for Fundamental Research and Development (2011CB612207), the Beijing Natural Science Foundation (2112006), and the German Research Foundation (SPP 1473-SO 1075/1-1).

Received: July 5, 2011
Published online: September 12, 2011

[1] A. Sleight, *Nature* **2003**, *425*, 674.
[2] J. R. Salvador, F. Gu, T. Hogan, M. G. Kanatzidis, *Nature* **2003**, *425*, 702.
[3] Y. Zhang, Z. Islam, Y. Ren, P. A. Parilla, S. P. Ahrenkiel, P. L. Lee, A. Mascarenhas, M. J. McNevin, I. Naumov, H. X. Fu, X. Y. Huang, J. Li, *Phys. Rev. Lett.* **2007**, *99*, 215901.
[4] J. Li, W. H. Bi, W. Ki, X. Y. Huang, S. Reddy, *J. Am. Chem. Soc.* **2007**, *129*, 14140.
[5] J. Chen, X. R. Xing, C. Sun, P. H. Hu, R. B. Yu, X. W. Wang, L. H. Li, *J. Am. Chem. Soc.* **2008**, *130*, 1144.
[6] T. A. Mary, J. S. O. Evans, T. Vogt, A. W. Sleight, *Science* **1996**, *272*, 90.
[7] X. G. Zheng, H. Kubozono, H. Yamada, K. Kato, Y. Ishiwata, C. N. Xu, *Nat. Nanotechnol.* **2008**, *3*, 724.
[8] S. Iikubo, K. Kodama, K. Takenaka, H. Takagi, M. Takigawa, S. Shamoto, *Phys. Rev. Lett.* **2008**, *101*, 205901.
[9] Y. W. Long, N. Hayashi, T. Saito, M. Azuma, S. Muranaka, Y. Shimakawa, *Nature* **2009**, *458*, 60.
[10] D. Das, T. Jacobs, L. J. Barbour, *Nat. Mater.* **2010**, *9*, 36.
[11] E. F. Wasserman, in *Handbook of Magnetic Materials: A Handbook on the Properties of Magnetically Ordered Substances*, Vol. *5*, (Eds: K. H. J. Bushow, E. P. Wohlfarth), Elsevier Science, The Netherlands **1990**, Ch. 3.
[12] K. Takenaka, H. Takagi, *Appl. Phys. Lett.* **2009**, *94*, 131904.
[13] S. Margadonna, K. Prassides, A. N. Fitch, *J. Am. Chem. Soc.* **2004**, *126*, 15390.
[14] A. E. Phillips, G. J. Halder, K. W. Chapman, A. L. Goodwin, C. J. Kepert, *J. Am. Chem. Soc.* **2010**, *132*, 10.
[15] Y. Sun, C. Wang, Y. C. Wen, K. G. Zhu, J. T. Zhao, *Appl. Phys. Lett.* **2007**, *91*, 231913.
[16] Y. Nakamura, K. Takenaka, A. Kishimoto, H. Takagi, *J. Am. Ceram. Soc.* **2009**, *92*, 2999.
[17] X. Y. Song, J. X. Zhang, M. Yue, E. D. Li, H. Zeng, N. D. Lu, M. L. Zhou, T. Y. Zuo, *Adv. Mater.* **2006**, *18*, 1210.
[18] X. Y. Song, J. X. Zhang, E. D. Li, N. D. Lu, F. X. Yin, *Nanotechnology* **2006**, *17*, 5584.
[19] Z. H. Sun, X. Y. Song, *Mater. Lett.* **2009**, *63*, 2059.
[20] M. Seyring, X. Y. Song, A. Chuvilin, U. Kaiser, M. Rettenmayr, *J. Mater. Res.* **2009**, *24*, 342.
[21] M. Seyring, X. Y. Song, M. Rettenmayr, *ACS Nano* **2011**, *5*, 2580.
[22] A. C. Larson, A. C. Von Dreele, Los Alamos National Laboratory Report No. LAUR086-748 **2000**.